Manipulation of visual information affects control strategy during a visuomotor tracking task

Bank, Paulina J.M.; Dobbe (student), L.R.M.; Meskers, Carel G M; de Groot, Jurriaan H.; de Vlugt, Erwin

DOI
10.1016/j.bbr.2017.04.056

Publication date
2017

Document Version
Final published version

Published in
Behavioural Brain Research

Behavioural Brain Research 329 (2017) 205–214

Contents lists available at ScienceDirect

Behavioural Brain Research

journal homepage: www.elsevier.com/locate/bbr

Research report

Manipulation of visual information affects control strategy during a visuomotor tracking task

Paulina J.M. Bank[a,*], Lucas R.M. Dobbe[b], Carel G.M. Meskers[c,d], Jurriaan H. de Groot[e], Erwin de Vlugt[b]

[a] Department of Neurology, Leiden University Medical Center, P.O. Box 9600, 2300 RC Leiden, The Netherlands
[b] Faculty of Mechanical, Maritime and Materials Engineering, Section of Biomechanical Engineering, Delft University of Technology, Mekelweg 2, 2628 CD Delft, The Netherlands
[c] Department of Rehabilitation Medicine, VU University Medical Center, P.O. Box 7057, 1007 MB Amsterdam, The Netherlands
[d] Research Institute MOVE, Van der Boechorststraat 7, 1081 BT Amsterdam, The Netherlands
[e] Department of Rehabilitation Medicine, Leiden University Medical Center, P.O. Box 9600, 2300 RC Leiden, The Netherlands

ARTICLE INFO

Keywords:
Visuomotor control
Visual feedback
Strategy
System identification
Neuromechanical parameters

ABSTRACT

Proper understanding of motor control requires insight into the extent and manner in which task performance and control strategy are influenced by various aspects of visual information. We therefore systematically manipulated the visual presentation (i.e., scaling factor and optical flow density) of a visuomotor tracking task without changing the task itself, and investigated the effect on performance, effort, motor control strategy (i.e., anticipatory or corrective steering) and underlying neuromechanical parameters (i.e., intrinsic muscle stiffness and damping, and proprioceptive and visual feedback). Twenty healthy participants controlled the left-right position of a virtual car (by means of wrist rotations in a haptic robot) to track a slightly curved virtual road (presented on a 60" LED screen), while small torque perturbations were applied to the wrist (1.25–20 Hz multisine) for quantification of the neuromechanical parameters. This visuomotor tracking task was performed in conditions with low/medium/high scaling factor and low/high optical flow density. Task performance was high in all conditions (tracking accuracy 96.6%–100%); a higher scaling factor was associated with slightly better performance. As expected, participants did adapt their control strategy and the use of proprioceptive and visual feedback in response to changes in the visual presentation. These findings indicate that effects of visual representation on motor behavior should be taken into consideration in designing, interpreting and comparing experiments on motor control in health and disease. In future studies, these insights might be exploited to assess the sensory-motor adaptability in various clinical conditions.

1. Introduction

Given that vision if reliable is dominant over the other senses in many situations [1,2] and strong connections exist between the visual and the motor system [3,4] proper understanding of motor control requires insight into the extent and manner in which task performance and control strategy are influenced by various aspects of visual information such as resolution intensity contrast optical flow density and predictability. Between different studies and experiments however the visual representation of the task is usually not controlled (e.g., screen size, resolution, distance between the participant and the screen, scaling factor of visual feedback, the degree of immersion (screen, virtual reality, augmented reality) etc. Hence it is assumed that variation in the visual representation of the task under study does not affect the motor control that is being studied. Insight into the effects of visual representation on motor behavior however is important for designing interpreting and comparing experiments on motor control in health and disease. In future studies these insights might be exploited to assess sensory-motor adaptability, which is essential for adequate interaction with the environment in daily life, in various clinical conditions.

Against this background, we hypothesized that visual representation of a task would affect motor control even if the task demands remained unchanged. We therefore systematically manipulated the visual pre-

Abbreviations: ANOVA, analysis of variance; ARMAX model, autoregressive moving average model; ECR, extensor carpi radialis muscle; FCR, flexor carpi radialis muscle; MVC, maximum voluntary contraction; RMSE, root mean square error; SEM, standard error of the mean; SIPE, system identification and parameter estimation

* Corresponding author.
E-mail address: p.j.m.bank@lumc.nl (P.J.M. Bank).

http://dx.doi.org/10.1016/j.bbr.2017.04.056
Received 20 February 2017; Received in revised form 25 April 2017; Accepted 28 April 2017
Available online 10 May 2017

sentation (i.e. scaling factor and optical flow density) of a visuomotor tracking task without changing the task itself and investigated the effect on performance, effort, motor control strategy, and underlying neuromechanical parameters. It was anticipated that a higher resolution and density of visual information (i.e. higher scaling factor [5,6] and higher optical flow density [7,8]) would provide more reliable visual information which in turn may contribute more to motor control (i.e. receive a higher weight in the sensory weighing of input signals [9]). Consequently higher scaling factor and higher optical flow density were expected to result in improved performance with lower effort and more anticipatory control.

2. Methods

The present study aimed to determine the effects of visual information (i.e., scaling factor and optical flow density) on task performance, effort, control strategy and underlying neuromechanical parameters during a visuomotor tracking task that was presented on a LED screen. Participants controlled the left-right position of a virtual car, by means of small flexion and extension movements of the wrist, in order to track a slightly curved virtual road. Task performance was defined by tracking accuracy. Effort and co-contraction were determined by the muscle activity, and the adopted control strategy was quantified in terms of the steering delay and corrective steering actions. Neuromechanical properties (i.e., intrinsic muscle stiffness and damping, and contributions of proprioceptive and visual feedback) underlying task performance and control strategy were quantified using System Identification and Parameter Estimation (SIPE) (e.g. [10–14]).

2.1. Participants

18 healthy adults (13 female; 16 right-handed; age 50–76 years) with normal or corrected to normal vision participated in the study. Participants had no known history of lesions or diseases of the nervous system, or other conditions associated with pain and/or limited sensory or motor function of the upper extremities. Informed consent was obtained from all individual participants included in the study. All procedures performed in this study were approved by the ethical committee of the Leiden University Medical Center and in accordance with the 1964 Helsinki declaration and its later amendments.

2.2. Measurement setup

Throughout the experiment, participants sat in a chair with their elbow flexed and their feet supported. On a 60" flatscreen LED TV (Sharp LC-60LE652E, Sharp Electronics Europe Ltd., Usbridge, UK) placed circa 1.5 m in front of the participant, a visuomotor tracking task was presented by means of a virtual car on an animated curved road in a virtual environment (D-flow software; Motekforce Link B.V., Amsterdam, The Netherlands). Participants had to control the left-right movements of the virtual car by means of flexion and extension movements of their right wrist (≈10° peak-to-peak movement amplitude). To this end, the forearm was placed in a haptic robot (Wristalyzer™; MOOG FCS Inc., Nieuw Vennep, The Netherlands), consisting of a vertically positioned servo-controlled motor (Parker SMH100 series) that only permitted flexion-extension movements of the wrist in the horizontal plane. The forearm was placed in the apparatus with thumb up and palm facing inward, and its position was restrained to prevent movements of the elbow. The rotation axis of the wrist was aligned with that of the motor such that movement of the motor was directly coupled to flexion-extension of the wrist. The distance between the handle (diameter 32 mm) and the forearm support was adjusted such that the handle fell in the crease between thumb and index finger (see Fig. 1). The robot's neutral position corresponded with the handle being aligned with the forearm.

2.3. Data collection procedure

Participants were instructed to control the left-right position of a virtual car (presented on the LED screen) by means of small flexion and extension movements of the wrist in order to track a slightly curved virtual road (see 2.4.1), while small torque perturbations were applied by the haptic robot (see 2.4.1). Two features of the visual scenery were manipulated to change the visual presentation of the task (Fig. 2), without affecting the task demands: (1) *scaling factor*, which concerned the scaling of the virtual car and the road as well as the scaling between movements of the wrist and those of the virtual car (3 levels: low, medium, and high; corresponding to 0.5, 1 and 2 times the 'default' scaling factor). With the default scaling factor, the virtual car and the road were circa 5 and 11 cm wide, respectively, and 1° of wrist movement corresponded to circa 4.5 cm displacement of the virtual car on the screen; with a higher scaling factor all objects in the virtual environment were larger and a given wrist movement resulted in larger movement of the virtual car; and (2) *optical flow density*, which was defined by the absence or presence of a virtual tunnel with textured walls (2 levels: low optical flow density (without tunnel) and high optical flow density (with tunnel); tunnel width circa 60 cm, 80 cm and 130 cm, respectively, in conditions with low, medium and high scaling factor). These manipulations were intended to have *no effect on the task demands*, e.g. in conditions with high scaling factor a given wrist movement resulted in twice as large movements of the virtual car (i.e., 1° of wrist movement corresponded to circa 9 cm of displacement of the virtual car), but the road (22 cm) and virtual car (10 cm) were also twice as wide.

All combinations of the abovementioned factors were tested. Hence, the experiment involved 6 conditions. The order of conditions was randomized between participants, and one trial (duration: 30 s) was performed per condition. Two blocks of three consecutive trials were presented. At the start and the end of each block, and during transitions between consecutive trials, scaling of the visual scenery changed linearly from one condition to the next in 10 s and changes in optical flow density were gradually introduced, i.e., the virtual tunnel (or its end) became visible in the distance and was approached within 5 s, such that the virtual car entered (or left) the virtual tunnel 5 s before the start of the actual trial. These gradual transitions provided sufficient time to adapt to the new condition. In specific, the three-trial blocks were separated by a 40-s pause during which stimulating performance feedback on the task was provided to motivate the participant (i.e., a score reflecting the percentage of time on the road, averaged over the three trials within that block).

A practice trial (medium scaling factor and low optical flow density) prior to the first experimental condition served to familiarize participants with the visuomotor tracking task. During the practice trial, a fixed set of perturbation powers was tested (in random order) to determine the appropriate power of the perturbation signal for each individual participant. To allow for application of linear modeling techniques in the SIPE analyses, we selected the power for which wrist rotations due to the exerted torques had a standard deviation of approximately 2° and coherence between perturbation torques and wrist rotations [15] was > 0.7 for all frequencies in the signal. The selected power of the perturbation signal varied between 0.07 (n = 12) and 0.08 (n = 6), which corresponded to maximum torques of 0.12 and 0.14 Nm, respectively. For each individual participant, the selected power was used for all conditions of the experiment.

2.4. Input and output signals

2.4.1. Input (task) signals

2.4.1.1. Visual. On the LED screen a virtual road was presented that served as visual input for the tracking task (X_{ref} in Figs. 3a, 4 and 5. It consisted of three (phase shifted) sinusoids in order to reduce the predictability of the road curvature and was defined as:

Fig. 1. Overview of the experimental setup, with a close-up top view of the arm positioned in the haptic robot.

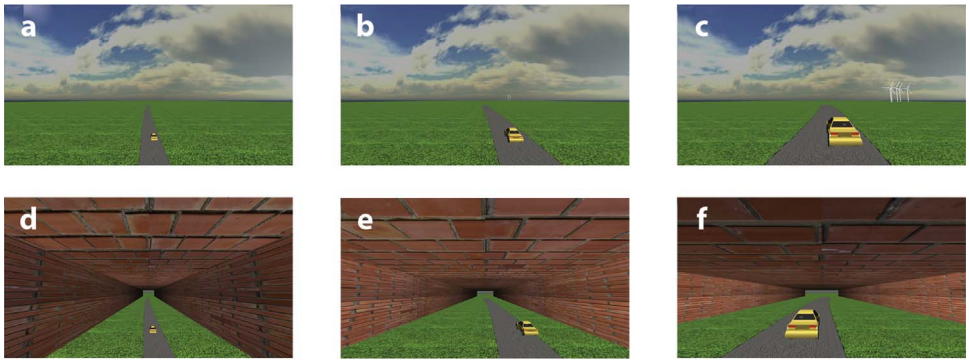

Fig. 2. Impression of the visual scenery in the six experimental conditions, with systematic manipulation of scaling factor (a,d: low; b,e: medium; and c,f: high) and optical flow density (a–c: low; d–f: high).

$$X_{ref} = 4\left[0.1\sin(2\pi f_1 t) + 0.4\sin\left(2\pi f_2 t - \frac{\pi}{3}\right) + 0.1\sin(2\pi f_3 t - 1.5\pi\right)] \quad (1)$$

with $f_1 = 0.2$ Hz and $f_2 = f_3 = 0.1$ Hz.

As a result, the visual task required voluntary steering movements up to 0.2 Hz at about 10° peak-to-peak movement amplitude to approximate linear conditions and thus allow for application of linear modeling techniques. In all conditions, a 1.25 s preview of the upcoming trajectory was provided.

2.4.1.2. Mechanical. The haptic robot applied unpredictable torque perturbations to the wrist to estimate the neuromuscular properties underlying task performance using SIPE [12]. The perturbation signal (T_D in Figs. 3b and 4) consisted of a repeating unpredictable 4-s multi-sine signal (full power spectrum over frequency bandwidth 1.25 – 20 Hz, with $\Delta f = 0.25$ Hz (i.e., 76 frequencies), maximum torque 0.14 Nm) with equal power per frequency and randomized phases (uniformly distributed between 0 and 2π radians). The lower boundary of perturbation frequencies was set at 1.25 Hz to avoid interference with voluntary steering (i.e., tracking movements up to 0.2 Hz and potential corrective movements up to a frequency of ca. 1 Hz [16]).

2.4.2. Output signals

2.4.2.1. Mechanical. Angular displacement of the haptic robot's handle (X) was measured using a high resolution angular encoder and wrist rotation torque (T) was measured using a force transducer mounted between the motor axis and the handle (see Fig. 3a and b for example signals). Positive values indicated flexion angles and torques of the hand to the handle, respectively. Position and torque outputs were digitized using a 16-bit A/D converter and subsequently imported to D-flow software (Motekforce Link B.V., Amsterdam, The Netherlands) for storage and for real-time control of the virtual car's movements (at 100 Hz). A first order filter ($\tau = 0.1$ s) was applied to the wrist's angular position signal to minimize the visual effects of high frequency torque perturbations. To quantify corrective steering (see 2.5.2), the raw angular position data were low-pass filtered (third order recursive Butterworth filter, 20 Hz) after offset correction. For SIPE analyses, the raw angular position and torque were up-sampled to 2048 Hz (by means of linear interpolation) to allow for synchronization with the applied perturbation signal. The synchronized signals were subsequently band-pass filtered (third order recursive Butterworth filter, 1.25–20 Hz) and down-sampled to 128 Hz to reduce computational effort.

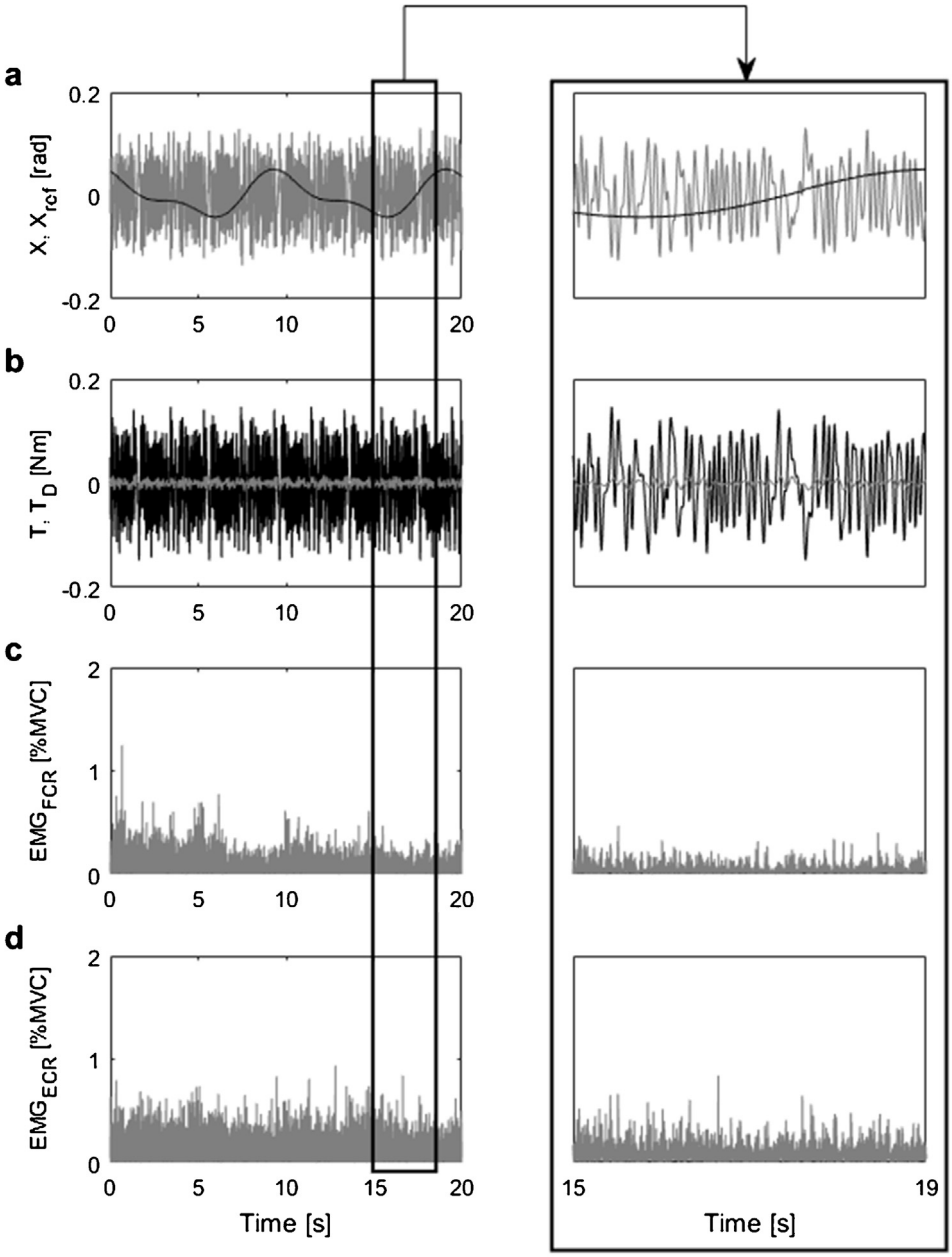

Fig. 3. Example of input signals (black) and output signals (grey) for a randomly selected subject. Input signals X_{ref} (visual; road position) and T_D (mechanical; torque perturbations); Output signals X (mechanical; angular displacement), T (mechanical; wrist rotation torque) and muscle activity (EMG amplitude envelope) obtained from the flexor carpi radialis (FCR) and extensor carpi radialis (ECR) muscles.

2.4.2.2. Muscle activity. Bipolar surface electromyography (EMG) was obtained from the flexor carpi radialis (FCR) and extensor carpi radialis (ECR) muscles of the tested arm. After preparation of the skin, disposable surface electrodes were positioned in the center of the muscle belly on the line from origin to insertion as determined by palpation. EMG signals were sampled at 2000 Hz, with 22 bits A/D conversion (Porti7 with 600 Hz low-pass filter; TMSi international BV, Oldenzaal, the Netherlands). EMG signals were filtered to remove movement artifacts (third order recursive Butterworth high-pass filter, 10 Hz), full-wave rectified and normalized to EMG values obtained during maximum voluntary contraction (MVC). Subsequently the EMG amplitude envelope was extracted by means of a third order recursive Butterworth 20 Hz low-pass filter (see Fig. 3c and d for an example).

2.5. Data analysis

Data analysis was performed using Matlab (The Mathworks Inc., Natick MA, version R2014a). The first 5 s of each trial were removed in order to eliminate any transient effects. To ensure that the length of the analyzed time series corresponded to an exact multiple of the repeating 4-s perturbation signal (required for SIPE purposes), all analyses were performed on the subsequent 20 s.

2.5.1. Task performance, effort and co-contraction

Task performance was defined as the percentage of time that participants were able to keep the center of the car between the boundaries of the road. Effort was quantified by means of the total muscular activity and was calculated at each time point as the sum of FCR and ECR EMG values. Co-contraction, which was defined as any activity in the normally silent antagonist muscle, was calculated at each

time point as the minimum value of EMG between the FCR and the ECR [17]. The obtained values were subsequently averaged per trial.

2.5.2. Control strategy: steering delay and corrective steering

Reactive steering, in which the actual track was delayed compared to the road (positive delay) and anticipatory steering, in which the actual track was ahead of the road (negative delay) were identified using a nonlinear least squares optimization algorithm that minimized the difference between the car position and the center of the road, with time as the optimization variable. Corrective steering was quantified by means of the power of the angular position data. P_{corr} (in %) was calculated as the relative power within the 0.3–1.2 Hz 'corrective steering' bandwidth (expressed as a percentage of total power within the 0.01–1.2 Hz 'voluntary steering' bandwidth). Ideally, the full power would be reflected in frequencies required for tracking the road (i.e., up to 0.2 Hz), but in reality, under- and overshoots in voluntary steering require corrective movements (up to a frequency of ca. 1 Hz in systems with a visual delay of 200–300 ms [16]).

2.5.3. System identification and parameter estimation

In order to quantify the underlying neuromuscular properties, the relation between the predefined torque perturbations and the resulting responses by the participant was first quantified by system identification methodology (SI, Section 2.5.3.1) and was subsequently broken down into physiologically meaningful parameters (PE; section 2.5.3.2). This two-stage procedure, which was performed for each participant in each condition, is described in the following sections. In the first stage (SI), a non-parametric model was fitted to the observed data to estimate the mechanical admittance of the wrist. In the second stage (PE), a linear neuromechanical model was used for parameterization of the estimated admittance into neuromechanical parameters.

2.5.3.1. Non-parametric system identification – admittance. Estimation of mechanical admittance of the wrist $H_{wrist}(f)$ was performed using a proven non-parametric procedure based on autoregressive moving average (ARMAX) models of the 8th order [18]. As the angular displacement is determined both by the human wrist and the manipulator dynamics (Fig. 4), the procedure consisted of two-stages. First, the total admittance between torque disturbance and wrist angle was estimated according to:

$$H_{T_DX} = \frac{X(k)}{T_D(k)} = \frac{H_{robot}}{1+(H_{wrist}*H_{robot})} \quad (2)$$

Second, the transfer function between torque perturbation and wrist reaction torque was estimated, being:

$$H_{T_DT} = \frac{T(k)}{T_D(k)} = \frac{H_{wrist}*H_{robot}}{1+(H_{wrist}*H_{robot})} \quad (3)$$

Subsequently, the wrist admittance was composed from Eqs. (2) and (3) as follows:

$$H_{wrist,ARMAX}(f) = \frac{H_{TDT}}{H_{TDX}} \quad (4)$$

Model estimations were based on the full bandwidth of the perturbation signal (1.25–20 Hz). However, because task-dependent adaptations of admittance are particularly evident at low frequencies [15], we also calculated the average gain of $H_{wrist,ARMAX}(f)$ of frequency points between 1.25 and 4.5 Hz (i.e., low-frequency wrist admittance; $Admittance_{<4.5Hz}$ for statistical analysis. The goodness of fit of the estimated ARMAX model was described by the Root Mean Square Error ($RMSE_{ARMAX}$) between the estimated wrist torque and the measured wrist torque.

2.5.3.2. Parametric system identification – neuromechanical parameters. A linear neuromechanical model was used for parameterization of the estimated admittance into neuromechanical parameters. Fig. 5 presents a schematic of the model, which was adopted from [4] and was extended to include a visual feedback loop (Supplemental Appendix A provides an in-depth description of the model components). The estimated neuromechanical parameter for H_P, i.e., passive wrist dynamics, was inertia (I). For H_{CE}, i.e., intrinsic properties of the contractile element, estimated parameters were damping (B) and stiffness (K), for H_{MS}, i.e., proprioceptive feedback, estimated parameters were velocity reflex gain k_v and time delay $\tau_{d,v}$, and for H_{vis}, i.e., visual feedback, estimated parameters were position feedback gain k_{vis} and time delay $\tau_{d,vis}$. Fixed parameters were used to describe the muscle activation dynamics (H_{act} with relative damping 0.7 and eigen-frequency f_0 = 2.5 Hz; [13]), an identified hardware delay (τ_{hw} = 0.135 s) and the first order filter that was applied to the wrist angular position signal prior to visualization on the LED screen (H_{vf} with τ_{vf} = 0.1 s). This model including reflexive velocity feedback and long-latency visual feedback was tested to be superior for parametric analysis over other combinations of afferent feedback (position, velocity and force) and visual feedback, based on high goodness of fit of the model and low variability of the estimated parameters (i.e., low $RMSE_{PM}$ and low nSEM; see next paragraph).

The model parameters were optimized in the frequency domain, using a nonlinear least squares optimization algorithm that minimized the error between the modeled wrist admittance $H_{wrist,model}(f)$ and the estimated $H_{wrist,ARMAX}(f)$ according to:

$$E(f) = \left| \log\left(\frac{H_{wrist,ARMAX}(f)}{H_{wrist,model}(f)} \right) \right| \cdot \frac{1}{f} \cdot \hat{\gamma}^2_{DX}(f) \quad (5)$$

with relatively higher weight being given to lower frequencies and to frequencies with a high coherence($\hat{\gamma}^2_{DX}(f)$) between the applied perturbation torque and measured wrist torque. Coherence was calculated according to [12]:

$$\hat{\gamma}^2_{DX}(f) = \frac{|\hat{S}_{DX}(f)|^2}{\hat{S}_{DD}(f) \cdot \hat{S}_{XX}(f)}, \quad (6)$$

in which $\hat{S}_{DX}(f)$ denotes the cross-spectral density of external torque perturbation $T_D(f)$ and wrist angle $X(f)$, $\hat{S}_{DD}(f)$ denotes spectral density

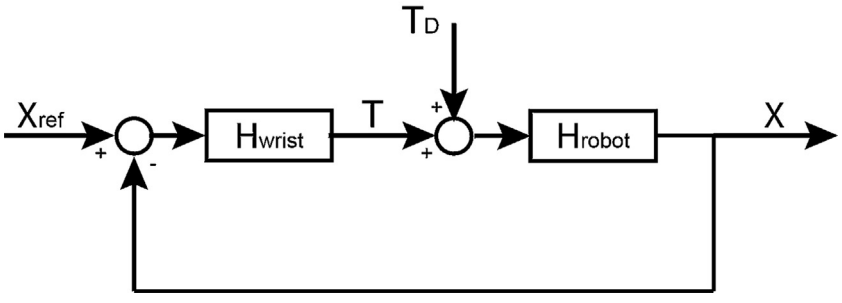

Fig. 4. The (simplified) control scheme, presenting the interaction of the human wrist (H_{wrist}) with the robot (H_{robot}) while minimizing the position of the car (X) with respect to the position of the road (X_{ref}) and being subjected to external torque perturbations (T_D).

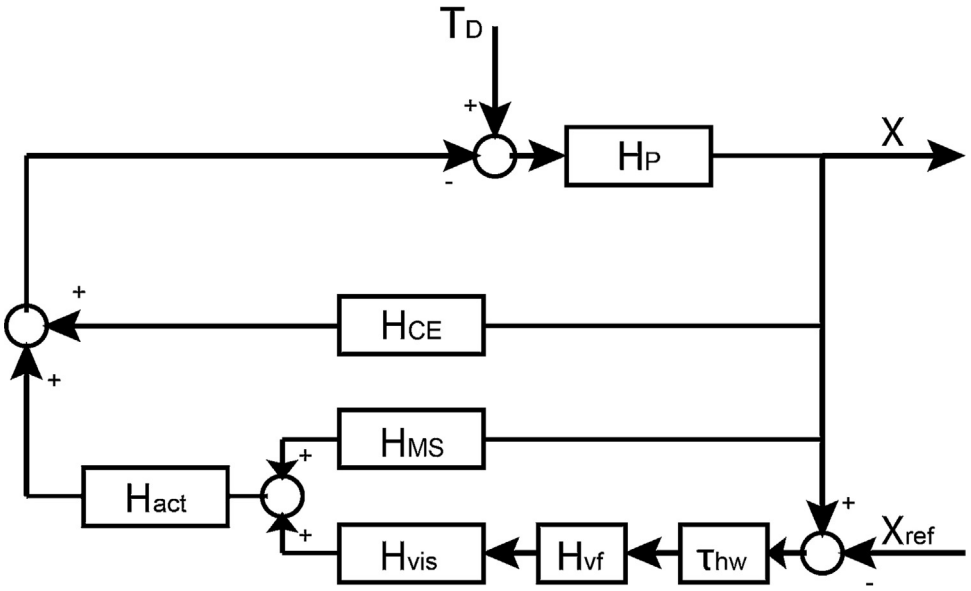

Fig. 5. Block scheme representation of the neuromechanical model. The human wrist (H_P) is perturbed mechanically by the torque perturbation signal (T_D) and perturbed visually by the position reference signal (X_{ref}). The intrinsic properties of the contractile element (H_{CE}), muscle spindle feedback (H_{MS}) and visual feedback (H_{vis}) are used to correct for these disturbances. H_{act} denotes the activation dynamics of (supra)spinal muscle force input signals. Visual feedback was delayed due to a hardware delay (τ_{hw}) and was filtered prior to visualization (H_{vf}). X is the measured output rotation of the wrist. An in-depth description of all model components can be found in Supplemental Appendix A.

of the external torque perturbation, and $\hat{S}_{XX}(f)$ denotes spectral density of the wrist angle. Coherence $\hat{\gamma}^2_{DX}(f)$ ranges from zero for systems with no linear relation to one for a linear system without noise. Optimization settings can be found in Supplemental Appendix B. The goodness of fit of the parametric model ($RMSE_{PM}$) was calculated in the frequency domain as the RMSE of $E(f)$. The role of parameters in the model was evaluated by means of the normalized standard error of the mean for the individual parameters (nSEM; normalization to the overall average estimated parameter value), with lower values indicating higher precision of estimation [19].

2.6. Statistical analysis

Statistical analysis was performed using IBM® SPSS® Statistics 20.0 (IBM Corp., Armonk NY).

Task performance was considered the primary outcome. Parameters related to effort (EMG_{sum}), co-contraction (EMG_{min}) and control strategy (steering delay and corrective steering P_{corr}), as well as the SIPE parameters ($Admittance_{<4.5Hz}$, and the neuromechanical parameters I, K,B, $k_{v,}$ $k_{vis,}$ $\tau_{d,v,}$ and $\tau_{d,vis}$) were considered higher resolution quantification of performance in terms of strategy and underlying mechanisms.

Normality curves were inspected and Kolmogorov-Smirnov tests were used to assess whether the data were normally distributed within each condition [20]. Substantial deviations from normality were observed for task performance, which could not be resolved by transformations due to a ceiling effect. After ^{10}log transformation of $RMSE_{ARMAX}$, $RMSE_{PM}$, $Admittance_{<4.5Hz}$ and P_{corr}, and after square root transformation of k_{vis} and $\tau_{d,vis}$, data were normally distributed in circa 90% of all conditions. Although transformed data were used for statistical analysis of these parameters, for reasons of clarity the untransformed data are presented in the Results.

Task performance was submitted to non-parametric Friedman's analysis of variance (ANOVA) to explore whether it was influenced by scaling factor and/or optical flow density. Wilcoxon signed-rank tests were used for post hoc analyses of significant effects. Parameters related to effort (EMG_{sum}), co-contraction (EMG_{min}) and control strategy (steering delay and corrective steering P_{corr}), as well as the goodness of fit ($RMSE_{ARMAX}$, $RMSE_{PM}$) and the SIPE parameters ($Admittance_{<4.5Hz}$ and the underlying neuromechanical parameters I, K,B, $k_{v,}$ $k_{vis,}$ $\tau_{d,v,}$ and $\tau_{d,vis}$) were each submitted to a repeated-measures ANOVA to evaluate the effects of visual presentation (scaling factor (3 levels) and optical flow density (2 levels) as within-subject factors). For all ANOVAs, degrees of freedom were adjusted if the sphericity assumption was violated [20] and effect sizes were quantified as partial eta squared (η_p^2). Post hoc analyses of significant effects ($p < .05$) were performed using two-tailed paired t-test with Bonferroni correction. All values are presented as mean ± standard deviation, except for performance and nSEM (values presented as median [interquartile range]).

3. Results

3.1. Task performance, effort and co-contraction

Across all participants and conditions, performance ranged from 96.6% to 100% (Fig. 6a). Task performance was slightly better with a high scaling factor (100% [99.7–100%]) than with a low scaling factor (99.8% [99.2–100%]), as was indicated by post hoc analysis of the significant effect of scaling factor ($\chi^2(2) = 7.96$, $p = .019$). Task performance was not influenced by optical flow density.

No significant main or interaction effects of scaling factor or optical flow density were observed for effort (EMG_{sum}; Fig. 6b) or co-contraction (EMG_{min}; Fig. 6c).

3.2. Control strategy: steering delay and corrective steering

From Fig. 6d and e it can be appreciated that steering delay and corrective steering were significantly influenced by scaling factor. Post hoc analysis of the main effect of scaling factor on steering delay ($F(2,34) = 99.4$, $p < .001$, $\eta_p^2 = .85$) indicated more anticipatory steering with higher scaling factor (low: −0.055 ± 0.041 vs. medium: −0.218 ± 0.091 vs. high: −0.425 ± 0.084 s; all $p < .05$). Similarly, post hoc analysis of the main effect of scaling factor on P_{corr} ($F(2,34) = 145.65$, $p < .001$, $\eta_p^2 = .90$) showed more corrective steering with higher scaling factor (low: 1.6 ± 0.6 vs. medium: 3.8 ± 2.7 vs. high: 14.4 ± 7.6%; all $p < .001$).

The significant main effect of optical flow density on P_{corr} ($F(1,17)$

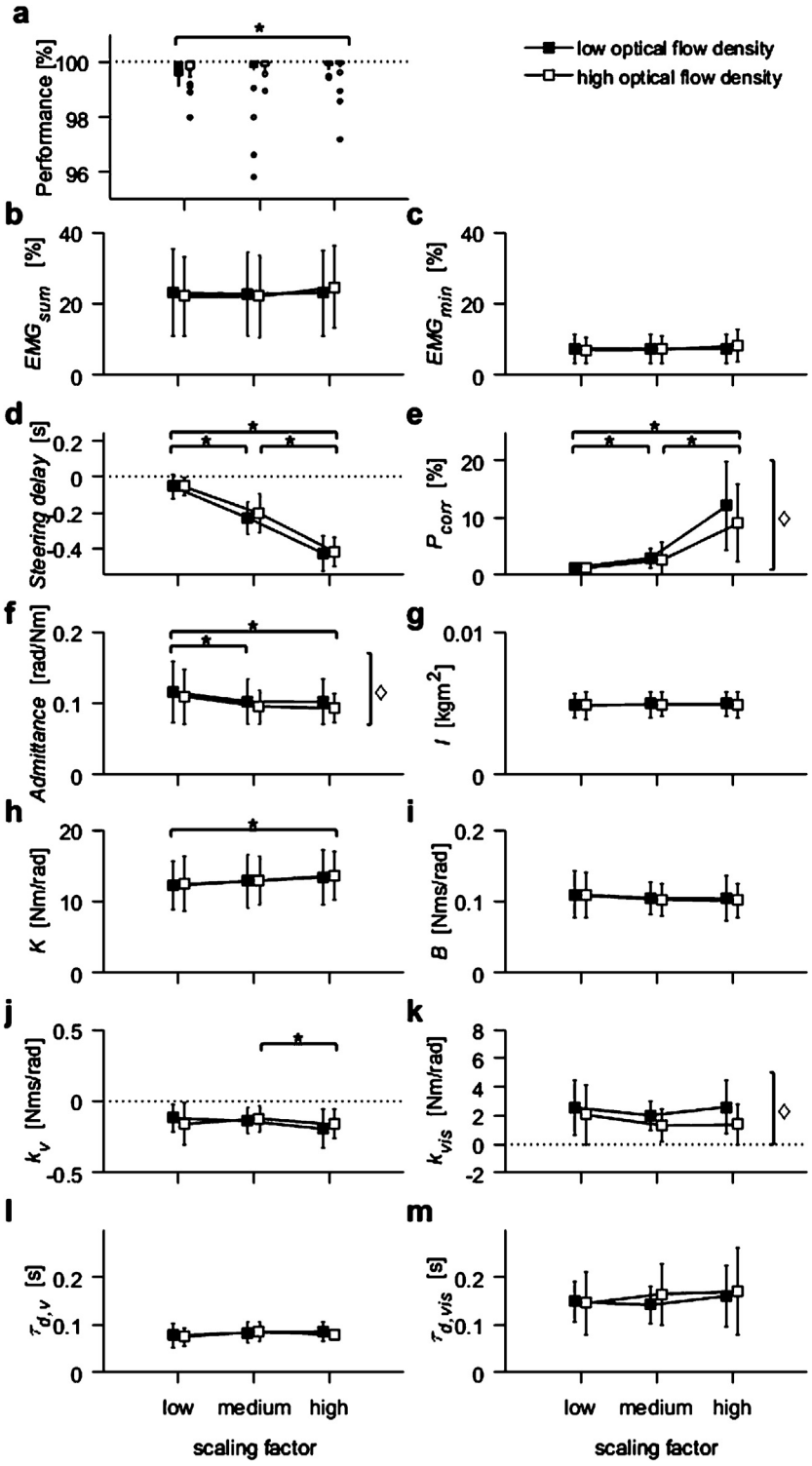

Fig. 6. Effects of scaling factor and optical flow density on (a) effort EMG_{sum} and (b) co-contraction EMG_{min}, on strategy, i.e., (c) steering delay and (d) corrective steering P_{corr}, on (e) low-frequency *Admittance* $_{<\ 4.5Hz}$, and on estimated neuromechanical parameters of the wrist, i.e., (f) inertia *I*, (g) intrinsic stiffness *K*, (h) intrinsic damping *B*, (i) proprioceptive reflex gain k_v, (j) visual feedback gain k_{vis}, (i) time delay of proprioceptive feedback $\tau_{d,v}$, and (j) time delay of visual feedback $\tau_{d,vis}$. Error bars represent standard deviations. * significant difference between scaling factors; ◊ significant main effect of optical flow density ($p < .05$).

$= 7.24$, $p = .015$, $\eta_p^2 = .30$) indicated slightly less corrective steering in the presence of a virtual tunnel (i.e., low optical flow density: 7.2 ± 3.6 vs. high optical flow density: 5.9 ± 3.3%).

3.3. System identification and parameter estimation

The system may be assumed to be linear as the overall mean coherence between perturbation torques and wrist rotations was 0.83 ± 0.08, with values > 0.7 in 94% of all cases. The averaged frequency-response-curve and corresponding coherence of each condition are presented in Supplemental Appendix C. In addition, a typical example of the fitting results is presented in Supplemental Appendix D.

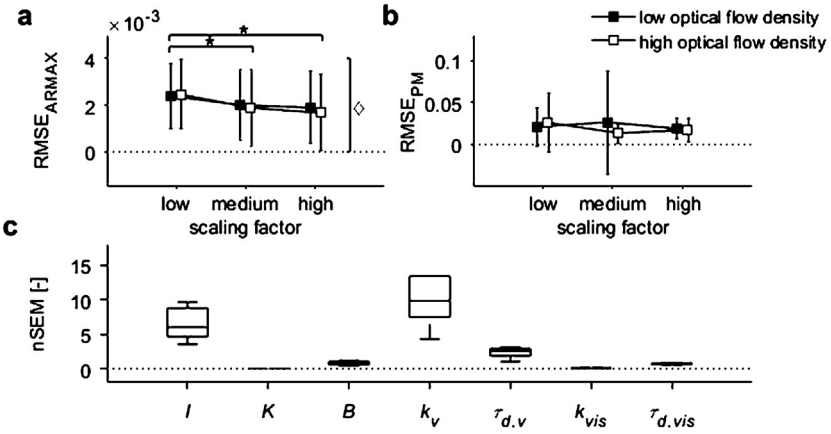

Fig. 7. Effects of scaling factor and optical flow density on (a) goodness of the non-parametric model fit, indicated by $RMSE_{ARMAX}$ (b) goodness of the parametric model fit, indicated by $RMSE_{PM}$ and (c) the normalized standard error of the mean for the individual parameters (nSEM; lower values indicate higher precision of estimation). * significant difference between scaling factors; ◊ significant main effect of optical flow density ($p < .05$).

3.3.1. Non-parametric system identification – admittance

Small $RMSE_{ARMAX}$ values were obtained for all participants, indicating that the non-parametric model fitted well to the observed data (Fig. 7a). $RMSE_{ARMAX}$ was slightly affected by the presence of a virtual tunnel (i.e., main effect of optical flow density $F(1,17) = 6.30$, $p = .023$, $\eta_p^2 = .27$; low: 0.0017 ± 0.0006 vs. high: 0.0016 ± 0.0006 rad/Nm), and was slightly higher for low scaling factor (0.0020 ± 0.0006 Nm/rad) compared to the medium and high scaling factor (0.0016 ± 0.0007 and 0.0014 ± 0.0007 Nm/rad; post-hoc analysis of the main effect of scaling factor ($F(2,34) = 17.31$, $p < .001$, $\eta_p^2 = 0.51$)).

Admittance $<_{4.5Hz}$ (Fig. 6f) decreased with medium and high scaling factor (0.099 ± 0.025 and 0.098 ± 0.025 rad/Nm) compared to low scaling factor (0.11 ± 0.04 rad/Nm), as was evidenced by post hoc analysis of the significant main effect of scaling factor ($F(2,34) = 6.28$, $p = .005$, $\eta_p^2 = .27$). The main effect of optical flow density ($F(1,17) = 5.25$, $p = .035$, $\eta_p^2 = .24$) indicated that *Admittance* $<_{4.5Hz}$ was slightly reduced in the presence of a virtual tunnel (i.e., low optical flow density: 0.107 ± 0.031 rad/Nm vs. high optical flow density: 0.100 ± 0.025 rad/Nm).

3.3.2. Parametric system identification – neuromechanical parameters

Although a significant main effect of scaling factor was observed for $RMSE_{PM}$ ($F(2,34) = 3.34$, $p = .047$, $\eta_p^2 = .16$), post-hoc analysis revealed no significant differences between the levels of scaling factor (Fig. 7b). Overall, precision of estimation was high for K, B, k_{vis} and $\tau_{d,vis}$, whereas higher nSEM values indicated lower precision of estimation for I, k_v and $\tau_{d,v}$ (Fig. 7c).

Stiffness K slightly increased when scaling factor increased ($F(2.34) = 4.94$, $p = .013$, $\eta_p^2 = .23$; Fig. 6h). Post hoc analysis revealed that K was significantly higher with the highest scaling factor compared to the lowest scaling factor (13.50 ± 3.44 vs. 12.29 ± 3.49 Nm/rad), but not significantly so when compared to the intermediate scaling factor (12.87 ± 3.40 Nm/rad). The scaling factor also influenced the proprioceptive reflex gain ($F(2,34) = 4.53$, $p = .018$, $\eta_p^2 = .21$; Fig. 6j), with a more negative k_v at the highest scaling factor (−0.18 ± 0.11 Nms/rad) compared to the intermediate scaling factor (−0.13 ± 0.09 Nms/rad; $p < .05$) and the lowest scaling factor (−0.14 ± 0.09 Nms/rad; n.s.). Increasing the optical flow density by means of a virtual tunnel resulted in a lower gain of visual feedback (low optical flow density: 2.38 ± 1.05 Nm/rad vs. high optical flow density: 1.58 ± 1.19 Nm/rad; Fig. 6k), as was evidenced by the main effect of optical flow density on k_{vis} ($F(1,17) = 9.79$, $p = .006$, $\eta_p^2 = .37$). No significant main or interaction effects of scaling factor and optical flow density were observed for damping ($B = 0.11$ ± 0.03 Nms/rad; Fig. 6i). As expected, no significant main or interaction effects were observed for the wrist inertia ($I = 0.0049$ ± 0.00085 kgm^2; Fig. 6g) and the neural time delays ($\tau_{d,v} = 0.081$ ± 0.013 s, Fig. 6l; and $\tau_{d,vis} = 0.155$ ± 0.032 s, Fig. 6m).

4. Discussion

This study showed that resolution and density of visual information (i.e., higher scaling factor and optical flow density) influence task performance and the control strategy that is adopted during a visuomotor tracking task in healthy adults. Task performance was high in all conditions, with tracking accuracy ranging from 96.6% to 100%; higher scaling factor was associated with a slight improvement of task performance. As expected, participants did adapt their control strategy in response to these systematic manipulations of the visual presentation of the task (i.e., without effect on task demands).

In specific, a higher scaling factor was associated with anticipatory steering (evidenced by a more negative steering delay) and more corrective steering actions (evidenced by higher P_{corr}). Probably, the higher scaling factor provided better visibility of the curvature of the upcoming road (allowing for anticipatory control) and better visibility of the deviations from the optimal position (allowing for improved use of visual information for the timing and magnitude of corrective steering actions [21]). The higher scaling factor was accompanied by a slightly higher stiffness K, which might either result from co-contraction (however, not supported by EMG data), or, more likely, faster alternation of agonist-antagonist activity. Proprioceptive reflex gain (k_v) was slightly more negative at the highest scaling factor, perhaps to retain stability and/or facilitate steering actions, whereas visual feedback gain (k_{vis}) was not affected by the scaling. Despite task performance already being close to 100% in the low-scaling condition, tracking accuracy was slightly better with a higher scaling factor, which is in line with other studies in which the error of position control [5] and force control [6] was visually amplified.

Effects of increasing the optical flow density were less pronounced. Whereas in other studies a higher optical flow density was associated with improved task performance [7,8], there was a possible ceiling effect on task performance in the present study obscuring the effect of optical flow density. The presence of a virtual tunnel with textured walls (i.e., high optical flow density) was associated with slightly less corrective steering actions (evidenced by lower P_{corr}) and a lower gain of visual feedback (k_{vis}). It can be speculated that the textured tunnel walls increased the reliability of velocity-related visual information, thereby making future predictions of the road position more reliable [22]. This may have reduced the need for corrective steering actions (resulting in lower P_{corr}) and may have resulted in less intense motor

actions in response to visual deviations from the reference position (indicated by lower k_{vis}). In addition, a small but significant reduction of admittance was observed (i.e., increased resistance), but this could not be substantiated by parameters related to co-contraction (i.e., no significant increase of muscle stiffness K, damping B or EMG_{min} was observed) or by parameters related to reflexive dynamics (i.e., no change in k_v). Optical flow density did not affect $RMSE_{PM}$, which suggests that the observed reduction of admittance was not likely attributable to reflexive dynamics that were not included in our model (i.e., reflexive position or force feedback).

Manipulation of visual information evoked changes in proprioceptive and visual feedback parameters of a neuromechanical model. To understand how this translates to physiological mechanisms, it is important to note that (1) the model provided a good description of the observed data (i.e., low $RMSE_{ARMAX}$ and $RMSE_{PM}$); (2) both the proprioceptive and visual feedback systems demonstrably contributed to the model fit (i.e., a comparison revealed that $RMSE_{PM}$ of the selected model was smaller than $RMSE_{PM}$ of models with other combinations of afferent feedback (i.e., position, velocity, and force) and visual feedback); (3) the added visual parameters provided a reliable contribution to the model (i.e., nSEM values for k_{vis} and $\tau_{d,vis} < 1$), however at the cost of a slightly reduced precision of estimating the proprioceptive parameters (higher nSEM values for k_v and $\tau_{d,v}$); and (4) the visual feedback parameter does *not* reflect proprioceptive feedback mechanisms, given that a time delay related to visualization of wrist movements (> 200 ms, by a hardware delay and a first order visual filter) was incorporated in the model (see Fig. 5) and the resulting visual pathway was too slow for proprioceptive feedback mechanisms [23]. Hence, it is evident that the modeled proprioceptive and visual feedback systems each contributed independently to the observed motor behavior.

With respect to the visual feedback, it is important to note that the value of k_{vis} was not directly affected by the visual manipulations because the scaling factor and optical flow density of this visual representation were not incorporated in the model. The gain of this long-latency position feedback loop (k_{vis}) thus reflects the magnitude of the motor response to a delayed, low-pass filtered representation of the angular deviation from a reference position. Although very small values of k_{vis} would be suggestive of a minimal contribution of visual information to motor control, higher values of k_{vis} do not necessarily implicate a larger contribution of visual information. For example, a slight reduction of k_{vis} (as observed in the present study for conditions with higher optical flow density), might also indicate less overcorrection of deviations from the reference position and thus indicate a more efficient use of the available visual information. The estimated time delay ($\tau_{d,vis} = 155$ ms) suggests that the provided visual feedback may be processed by the so-called voluntary reaction-time response (120–180 ms), which is mediated by the cortex and the spinal cord [23]. With respect to the proprioceptive feedback, the small values for k_v suggest that reflexive proprioceptive feedback was suppressed, presumably to retain stability in the presence of force perturbations at the eigenfrequency of the wrist joint [12,24]. The observed negative values for k_v are suggestive of an inhibitory feedback mechanism, where excitatory proprioceptive feedback might have been expected. Similar values, however, have been reported in position control tasks [15,24,25] and were suggested to have a stabilizing effect in combination with force feedback mechanisms. Studies in the cat have suggested that negative reflexive gains may arise from an inhibitory effect on Ia afferent input due to presynaptic inhibition [26] and an inhibitory effect on Ib afferent input (i.e., muscle force) due to shared interneural circuits [27]. The estimated time delay ($\tau_{d,v} = 80$ ms) suggest that the proprioceptive feedback was predominantly mediated by a long-latency response, which can be modulated by supraspinal steering commands and may be more flexible to task instructions or other sources of sensory information than spinal short-latency responses (approximate delay 30 ms) [23]. It may be speculated that, in the present study, these long-latency responses were used to facilitate steering actions (e.g., give way to perturbations in the extension direction for extension movements and vice versa).

In order to study the role of visual feedback we added visual feedback into a neuromechanical feedback model [13] and used this model for time-invariant 'steady state' analysis of motor behavior in different visual environments. In future studies, it would be interesting to explore the potential use of time-variant analyses [28] to gain insight in the dynamics of changes in control strategy, e.g., during the gradual transition from one condition to the next. Hypothetically, such time-variant analyses could also be used to validate the visual parameter that was added to the neuromechanical model, since the contribution of visual feedback would be expected to drop when visual feedback of the virtual car suddenly disappears. In future studies, it is important to minimize the time delay in the mechanical-visual interaction, since high time delays pose limitations to the potentially evoked steering intermittency of participants [16]. This is highly undesirable in the study of dynamic behavior in tracking tasks. Moreover, the suppression of proprioceptive reflexes may be avoided by applying reduced power to the higher frequencies in the perturbation signal [29]. Alternative approaches using predictive simulation models might contribute to understanding of mechanisms underlying the observed behavior.

Before drawing general conclusions from the current results, it should be considered that this study was conducted in elderly participants to match the age of patients with neurologic disorders such as stroke, which are associated with impaired motor adaptability. The present results cannot be unreservedly generalized to younger persons, because elderly might use strategies that are quite distinct [30]. Moreover, it remains to be investigated whether the (adaptations of) control strategies that were observed in this study during a relatively novel tracking task, are also applicable to more automatic behaviors [31].

In conclusion, the present study showed that systematic manipulations of visual presentation (scaling factor and optical flow density) that did not affect task demands did have influence on performance, control strategy and the use of proprioceptive and visual feedback. The implications of these findings are twofold. On one hand, one must be aware that the way of presenting visual information may have (possibly unwanted) effects on the motor behavior being investigated. In designing, interpreting and comparing experiments, this should thus be taken into consideration. On the other hand, understanding of the extent and manner in which visual information influences motor behavior can be exploited to assess the sensory-motor adaptability in health and disease. Manipulation of visual information and evaluation of visual and proprioceptive feedback characteristics, as described in this study, thus provides opportunities for high resolution quantification of (the lack of) motor adaptability in patients, for the purpose of diagnosis as well as tailored training.

Conflicts of interest

The authors declare that they have no conflict of interest.

Funding

This work is part of the research programme IMDI Neurocontrol (NeurAS project 10-10400-98-008) financed by the Netherlands Organisation for Health Research and Development. The funding party played no role in the study design, in the collection, analysis and interpretation of data, in the writing of the report, or in the decision to submit the article for publication.

Appendix A. Supplementary data

Supplementary data associated with this article can be found, in the online version, at http://dx.doi.org/10.1016/j.bbr.2017.04.056.

References

[1] F.B. Colavita, Human sensory dominance, Percept. Psychophys. 16 (1974) 409–412, http://dx.doi.org/10.3758/bf03203962.
[2] D. Hecht, M. Reiner, Sensory dominance in combinations of audio, visual and haptic stimuli, Exp. Brain Res. 193 (2009) 307–314, http://dx.doi.org/10.1007/s00221-008-1626-z.
[3] M.A. Goodale, A.D. Milner, Separate visual pathways for perception and action, Trends Neurosci. 15 (1992) 20–25.
[4] M.M. Veerman, E. Brenner, J.B. Smeets, The latency for correcting a movement depends on the visual attribute that defines the target, Exp. Brain Res. 187 (2008) 219–228, http://dx.doi.org/10.1007/s00221-008-1296-x.
[5] A. Beuter, H. Haverkamp, L. Glass, L. Carriére, Effect of manipulating visual feedback parameters on eye and finger movements, Int. J. Neurosci. 83 (1995) 281–294.
[6] S.L. Hong, K.M. Newell, Visual information gain and the regulation of constant force levels, Exp. Brain Res. 189 (2008) 61–69.
[7] I.R. Johnston, G.R. White, R.W. Cumming, The role of optical expansion patterns in locomotor control, Am. J. Psychol. 86 (1973) 311–324.
[8] M. Berntsen, M. Mulder, M.v. Paassen, Modelling human visual perception and control of the direction of self-motion, Proceedings of the AIAA Modeling and Simulation Technologies Conference and Exhibit, San Francisco, CA, 2005.
[9] M.O. Ernst, M.S. Banks, Humans integrate visual and haptic information in a statistically optimal fashion, Nature 415 (2002) 429–433 6870.
[10] R.E. Kearney, I.W. Hunter, System identification of human joint dynamics, Crit. Rev. Biomed. Eng. 18 (1990) 55–87.
[11] L.Q. Zhang, W.Z. Rymer, Simultaneous and nonlinear identification of mechanical and reflex properties of human elbow joint muscles, IEEE Trans. Biomed. Eng. 44 (1997) 1192–1209.
[12] F.C. van der Helm, A.C. Schouten, E. de Vlugt, G.G. Brouwn, Identification of intrinsic and reflexive components of human arm dynamics during postural control, J. Neurosci. Methods 119 (2002) 1–14.
[13] A.C. Schouten, W. Mugge, F.C. van der Helm, Nmclab, a model to assess the contributions of muscle visco-elasticity and afferent feedback to joint dynamics, J. Biomech. 41 (2008) 1659–1667, http://dx.doi.org/10.1016/j.jbiomech.2008.03.014.
[14] C.G. Meskers, J.H. de Groot, E. de Vlugt, A.C. Schouten, Neurocontrol of movement: system identification approach for clinical benefit, Front. Integr. Neurosci. 9 (2015) 48, http://dx.doi.org/10.3389/fnint.2015.00048.
[15] W. Mugge, D.A. Abbink, A.C. Schouten, J.P. Dewald, F.C. van der Helm, A rigorous model of reflex function indicates that position and force feedback are flexibly tuned to position and force tasks, Exp. Brain Res. 200 (2010) 325–340, http://dx.doi.org/10.1007/s00221-009-1985-0.
[16] R.C. Miall, J.K. Jackson, Adaptation to visual feedback delays in manual tracking: evidence against the smith predictor model of human visually guided action, Exp. Brain Res. 172 (2006) 77–84, http://dx.doi.org/10.1007/s00221-005-0306-5.
[17] N. Malfait, T.D. Sanger, Does dystonia always include co-contraction? A study of unconstrained reaching in children with primary and secondary dystonia, Exp. Brain Res. 176 (2007) 206–216, http://dx.doi.org/10.1007/s00221-006-0606-4.
[18] E. de Vlugt, A.C. Schouten, F.C. van der Helm, Quantification of intrinsic and reflexive properties during multijoint arm posture, J. Neurosci. Methods 155 (2006) 328–349, http://dx.doi.org/10.1016/j.jneumeth.2006.01.022.
[19] L. Ljung, System Identification: Theory for the User, Prentice Hall PTR, 1999.
[20] A. Field, Discovering Statistics Using SPSS, Sage Publications, London, UK, 2009.
[21] R.C. Miall, D.J. Weir, J.F. Stein, Intermittency in human manual tracking tasks, J. Mot. Behav. 25 (1993) 53–63, http://dx.doi.org/10.1080/00222895.1993.9941639.
[22] D.M. Wolpert, Z. Ghahramani, Computational principles of movement neuroscience, Nat. Neurosci. (3 Suppl) (2000) 1212–1217, http://dx.doi.org/10.1038/81497.
[23] R.A. Schmidt, C.A. Wrisberg, Motor Learning and Performance: A Situation-Based Learning Approach, Human Kinetics, Champaign, IL, 2008.
[24] A.C. Schouten, E. de Vlugt, J.J. van Hilten, F.C. van der Helm, Quantifying proprioceptive reflexes during position control of the human arm, IEEE Trans. Biomed. Eng. 55 (2008) 311–321, http://dx.doi.org/10.1109/tbme.2007.899298.
[25] E. De Vlugt, A.C. Schouten, F.C. van der Helm, Adaptation of reflexive feedback during arm posture to different environments, Biol. Cybern. 87 (2002) 10–26.
[26] E. Jankowska, D. McCrea, Shared reflex pathways from ib tendon organ afferents and ia muscle spindle afferents in the cat, J. Physiol. 338 (1983) 99.
[27] E. Brink, E. Jankowska, D. McCrea, B. Skoog, Inhibitory interactions between interneurones in reflex pathways from group ia and group ib afferents in the cat, J. Physiol. 343 (1983) 361.
[28] S. van Eesbeek, F.C.T. van der Helm, M. Verhaegen, E. de Vlugt, LPV subspace identification of time-variant joint impedance, in: B. He, M. Akay (Eds.), Proceedings of the 6th International IEEE/EMBS Conference on Neural Engineering. IEEE, Piscataway, USA, 2013, pp. 343–346.
[29] W. Mugge, D.A. Abbink, F.C. van der Helm, Reduced power method: how to evoke low-bandwidth behaviour while estimating full-bandwidth dynamics, Proceedings of the IEEE 10th International Conference on Rehabilitation Robotics, Noordwijk, The Netherlands, 2007, pp. 575–581.
[30] N.L. Goggin, H.J. Meeuwsen, Age-related differences in the control of spatial aiming movements, Res. Q. Exerc. Sport 63 (1992) 366–372.
[31] J.A. Taylor, J.W. Krakauer, R.B. Ivry, Explicit and implicit contributions to learning in a sensorimotor adaptation task, J. Neurosci. 34 (2014) 3023–3032.